Ultrasonic Phosphate Bonding of Nanoparticles

*David C Bassett, Geraldine Merle, Bruce Lennox, Reza Rabiei, François Barthelat, Liam M Grover, and Jake E Barralet**

New methods to assemble nanoparticulate materials are required to exploit the third dimension, creating functionality whilst also minimising contamination of the environment and end users. Most nano-assembly techniques either yield fragile materials formed through electrostatic or Van der Waals interactions or are adapted from macro and microscale joining techniques requiring heat to cause melting or solid state diffusion, which in turn can alter the nanostructure. Here we report our discovery that low intensity ultrasound-induced radicals interact with surface adsorbed orthophosphate to bond nanoparticles with high mechanical strength.

Collapse of sonically generated cavitation bubbles can damage materials by causing pitting.[1] This process and the associated generation of radicals are employed in chemical and particulate syntheses to accelerate reactions and alter the shape, size and phase of the product and efficiency of reactions.[2] Here we report the unexpected finding that exposure of orthophosphate-coated nanoparticulate xerogels to low power (0.2–1.4 W cm^{-2}) ultrasound led to irreversible agglomeration to form durable mesoporous assemblies.

Because of the colloidal nature of nanoparticles, avoiding human exposure following contamination of the workplace and environment is challenging.[3] Granulation potentially offers a safer way to handle nanoparticles, but only if the granules are both durable and functional. Currently the most employed method to assemble nanoparticles into mesoporous materials is by gelation of colloids through in situ synthesis or liquid removal, followed by drying at ambient or supercritical pressure to make xero- and aerogels, respectively.[4] Capillary stresses generated upon aqueous meniscus formation in nanopores are typically 100–200 MPa,[5] however these gels are mechanically weak having tensile strengths of typically only 150–300 kPa.[6] Consequently they are destroyed by even trace amounts of liquid which has severely limited the environments in which these gels can function. Prior improvements include combination with a tougher polymer, however this approach is not ideal since this occludes nanoporosity, or sintering which increases the particle size and hence reduces the available surface area[7] and may not be applied to thermally unstable or hydrated materials.

Ultrasound combined with an organic templating agent has previously been reported to synthesise ≈200 nm mesoporous titania particles via a calcination step by fusion of the constituent nanoparticles but was accompanied by a large reduction in surface area.[8] Ultrasonic welding of solid metallic and plastic components is well known and relies on either self-mating of metals following fragmentation of surface oxides or friction induced melting of plastics. High power (40–50 W cm^{-2}) ultrasound has been reported to fuse metallic (Au, Ag, Zn, Ni, Mo, Cr, Sn and Fe) nanoparticles[9] by local heating from inter-particle collisions, presumably assisted by nanometer-size related melting point suppression reported to be in the order of up to 900 °C.[10] Reports of ultrasonic mediated assembly of ceramics are scarce, however, fusion between 200 nm glassy silica particles in water induced by high power (100 W cm^{-2}) ultrasound has been reported.[11] These weak agglomerates appeared transiently and re-fragmented upon continued irradiation. Studies of silica nanoparticle size identified a critical threshold of 200 nm below which fusion did not occur. It was proposed that this was because smaller particles lacked sufficient kinetic energy for silicate bonding between the particles.[12]

When a wide variety of nanopowders, dispersed into slurries in a sodium phosphate solution and air dried to form phosphate-treated xerogels (PTX), were exposed to low power ultrasound, they formed microscale (≈200 μm) aggregates that we term phosphate bonded mesoporous microparticles (PBM). This was in stark contrast to phosphate free control (PFC) xerogels that simply fragmented within a few minutes. A wide variety of materials and dissimilar material combinations could be assembled using this technique without sacrificing functional properties. By way of illustration of the wide applicability of the method, we built 1 mm thick porous functional electrodes of the water splitting catalyst cobalt phosphate (CoPi),[13] which is both hydrated and amorphous, and composited this material with 0.3 wt% carbon nanotubes (CNT). This 3D

Dr. D. C. Bassett, Dr. G. Merle, Prof. J. E. Barralet
Faculty of Dentistry, McGill University
Montreal, H3A 2B2, Canada
E-mail: jake.barralet@mcgill.ca
Prof. B. Lennox
Department of Chemistry
Faculty of Science
McGill University
Montreal, H3A 2K6, Canada
Dr. R. Rabiei, Prof. F. Barthelat
Department of Mechanical Engineering
Faculty of Engineering, McGill University
Montreal, H3A 0C3, Canada
Dr. L. M. Grover
School of Chemical Engineering
University of Birmingham
Birmingham, B15 2TT, Great Britain
Dr. D. C. Bassett
Department of Physics
Norwegian University of Science and Technology
Trondheim, 7491, Norway
Prof. J. E. Barralet
Department of Surgery
Faculty of Medicine
McGill University
Montreal, Canada

DOI: 10.1002/adma.201301818

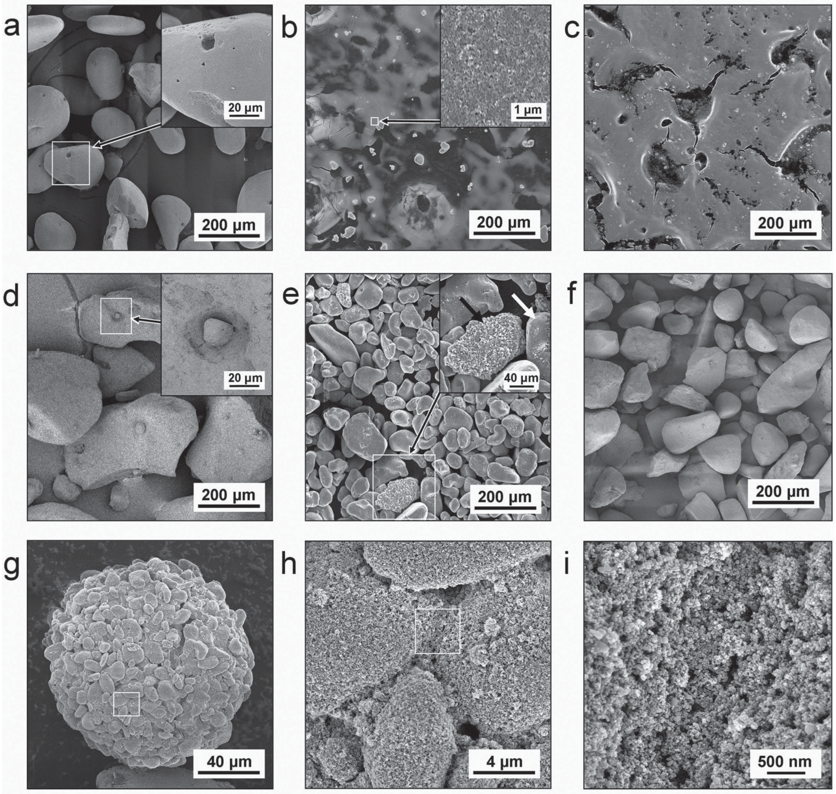

Figure 1. Scanning electron micrographs of TiO_2 PFC showing gradual disintegration after a) 5 mins b) 30 mins and c) 60 mins ultrasound treatment, and (d-f) TiO_2 PTX at the same timepoints. Inserts in a and d show surface details of the cavitation pits. Insert in e is a high magnification SEM of a PBM intermediate. The black arrow points to a microparticle consisting of rounded agglomerates of phosphate bonded gel fragments and the white arrow indicates a homogeneous and presumably 'mature' PBM in which the individual particles have consolidated but rough surface texture is still evident. Closer inspection of the intermediate stage PBM revealed that the individual particles from which they were assembled were clearly discernible (g), inter-particle bridges were formed from nanoparticulate gel (h), however the nanostructure appeared homogeneous in both particles and bridges (i)

electrode greatly exceeded the inherent efficiency limit of 2D CoPi electrodeposited films caused by electrical conductivity and mass transport which are significant at film thicknesses above 1 µm.[13b,14]

Following 5 min ultrasound exposure, both PFC and PTX TiO_2 gel particles had become rounded (cf. **Figure 1**a,d), and showed evidence of surface pitting. After 15 min the PFC had mostly disintegrated into a colloidal suspension that dried as a gel on the sample stub, (Figure 1b) yet PTX comprised two morphologies of microparticles 50–100 µm in dimension; one was smooth and apparently homogeneous (Figure 1e, white arrow), the other consisted of agglomerates of 3–10 µm gel particles (Figure 1e, black arrow). It appeared that these hierarchically arranged microparticles, themselves consisting of rounded agglomerates of 3–10 µm gel particles (Figure 1e, g-i), were an intermediate stage in the formation of PBM. Closer examination revealed that they were homogeneous at the nanoscale, however the original smaller microparticles from which they were comprised could still be distinguished (Figure 1h). Intriguingly, although these intermediates were clearly formed by particle-particle collision they appeared to have fused plastically since there was no evidence of any angular or flat surfaces normally associated with brittle fracture (Figure 1i). High magnification of the nanoparticulate gel between these smaller subunits did not indicate any gross change in density or primary particle size. This assembly could be due to either a process analogous to plastic deformation previously observed in ceramic particle impaction events[15] or following isostatic compression of silica aerogels,[16] or a thermally induced reversible gelation as has been treated theoretically[17] and observed in an inorganic pyrophosphate gel system.[18] After 60 min the PFC had completely disintegrated (Figure 1c), whereas PTX derived microparticles treated for 60 min had grown in size to ≈200 µm and appeared similar to each another (Figure 1f).

Several materials and their combinations could be assembled into PBM such as silver and silver-nanocarbon composites, nickel oxide, tungsten- and titania-hydroxyapatite composites as well as titania-CNT composites as shown in **Figure 2**; note that no phase changes were detected after treatment (Figure S1, Supporting Information). Their evolution was broadly similar as described for titania, however differences were found in the size and yield of particles formed. There was only a small reduction (average ca. 5%) in surface area between PTX and PBM particles as measured by BET (Table S1). Adsorption–desorption isotherms (Figure S2) demonstrated a narrow and steep hysteresis loop at high relative pressures. Following PBM formation, the hysteresis loop shifted slightly to higher relative pressures indicating a coarsening of nanoporosity. Pore size and volume approximation indicated a loss in pores 3–10 nm in size and a reduction in pores 10–25 nm in diameter upon PBM formation. Mercury porosimetry however did not reveal any changes in pore size distribution between 10–100 nm for titania or hydroxyapatite PBM (Figure S3).

Wet PBM were at least four times stronger than the PTX from which they were formed in all samples measured, and in some instances the strength of the xerogels could not even be determined since they fragmented upon contact with water or during sample manipulation into the measuring position (Figure 2a and Table S1). Tungsten PBM appeared to be an exception since it fragmented in water, but was 1.7 MPa in ethanol. Stability was assessed by dynamic light scattering (DLS) counts of water in which PBM were refluxed for an hour or after repeated cycles of drying and wetting (Figure S4). No nanoparticle generation was observed by DLS which was confirmed by ultracentrifuging the supernatant and examination using transmission electron microscopy (data not shown). Mechanical properties also remained unaltered by this procedure (Figure 2a).

Adv. Mater. 2013,
DOI: 10.1002/adma.201301818

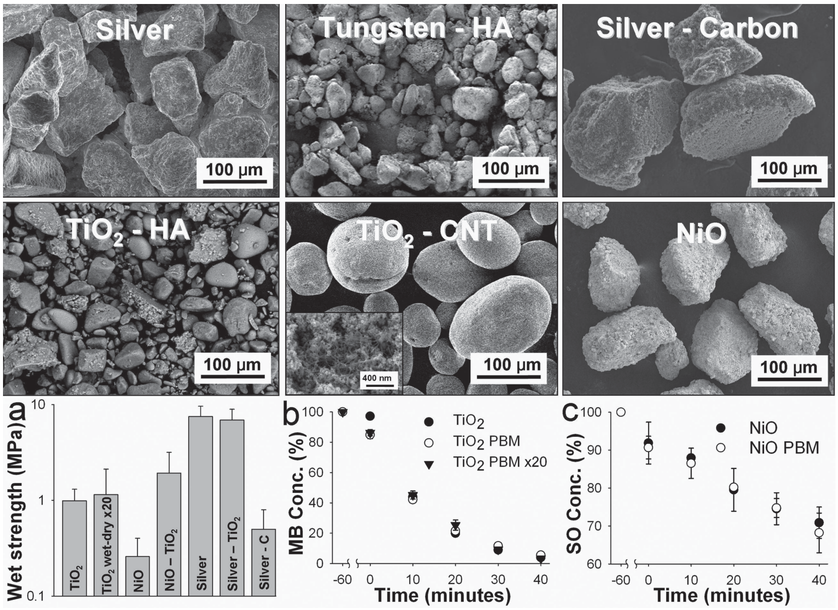

Figure 2. Scanning electron micrographs of washed PBM and composites (HA–hydroxyapatite, CNT–carbon nanotubes). a) Tensile strengths of PBM in water. TiO_2 wet-dry was repeatedly dried and rehydrated for 20 cycles and measured again. b) Photocatalytic activities as determined by the degradation of methylene blue (MB) under UV irradiation of: colloidal dispersion of TiO_2 nanopowder, TiO_2 PBM and TiO_2 PBM after 20 repeated photocatalytic activity tests (TiO_2 PBM X20) showing no loss in activity. c) Photocatalytic activity of NiO compared to NiO PBM under simulated solar irradiation as determined by the degradation of safranin O (SO).

PBM formation was found to be dependent upon H· but not OH· radicals since ultrasound exposure of PTX in the presence of H· scavengers resulted in complete fragmentation similar to PFC samples (Figure 1b,c), whereas PBM assembly was unaffected by the presence of OH· scavengers (Figure S5). H· scavenger efficiency was confirmed by KI oxidation dosimetry[19] (SE_{KI}) which was greatly reduced from 64.0 ± 5.1 to 3.7 ± 0.9 pmol J^{-1} with the addition of chloride ions, but only to 48 ± 3.5 pmol J^{-1} when sucrose was added as an OH· scavenger.

Careful displacement of air from dry PTX by wicking water in and leaving a gas 'escape route', rather than full liquid immersion which trapped bubbles in the gel, eliminated surface cavitation and subsequent PBM formation and identical results were obtained by placing the PTX under vacuum to expel the entrapped air prior to wetting. Therefore, localization of cavitation events at the xerogel surface and the generation of H· radicals seemed to be required for PBM formation. H· radicals are known to be extremely short-lived[20] and if they are involved in the strengthening of these gels they would need to be generated at the particles' surface in order to modify it. In addition to water, isopropyl alcohol (IPA) and glacial acetic acid could be used to form PBM whereas toluene and DMSO were not suitable. A common feature of the effective solvents appeared to be their protic and polar nature.

Having established that a phosphate coating was essential for PBM formation, an optimum concentration of 5 wt% was observed to give the highest yield of TiO_2 PBM (Figure S6). This amount corresponds to a theoretical phosphate coverage of ≈20% of the available surface. No evidence of crystalline sodium phosphate was detected through diffraction or electron microscopy in either PTX or PBM. After PBM formation with PTX containing 5% orthophosphate, the quantity of phosphate in the PBM reduced to 3 wt%, measured using inductively coupled plasma optical emission spectrometry (ICP-OES), suggesting some dissolution prior to bonding. The degree of protonation of orthophosphate was negligible since PBM formation could be replicated with phosphoric acid as well as mono and di sodium acid phosphates. However, substitution of 5 wt% orthophosphate in this process with 5 wt% sodium pyro-, tri- and poly-phosphates, nitrate or sulphate salts did not result in the formation of visible PBM and at this scale and fragmentation behaviour appeared to be identical to PFC. In exploring possible reactions of trisodium phosphate with ultrasound in IPA, we found that there were changes in the hydration and protonation of this salt (Figure S7), but no conversion to crystalline pyro- or poly-phosphate phases was detected.

We tested the hypothesis that localized heating, thought to occur during cavitation,[21] could have melted the surface adsorbed phosphates into a glassy polyphosphate phase[22] that fused the nanoparticles together. Titania PTXs made with either sodium or potassium phosphate were heated in a furnace to form Graham's or Kurrol salt glasses, respectively on the surface of the nanoparticles.[22] 0.6% phosphate yielded sufficient glass to fuse the xerogel into a monolith that could withstand handling, but when these were added to water the particles disintegrated in all cases (Figure S8).

PBM could be formed using either 20 or 42 kHz ultrasound; there was no difference in SE_{KI} at either frequency at 0.9 W cm^{-2} power, (65.7 ± 8.0 vs. 64.0 ± 5.1 pmol J^{-1},respectively) in good agreement with previous studies.[19] Lowering the ultrasonic power below 0.9 W cm^{-2} resulted in slower formation of PBM down to 0.2 W cm^{-2}, after which formation was prevented altogether. However, increasing it to above 1.4 W cm^{-2} caused fragmentation of PTX without assembly into PBM, likely because at this power the PBM was too weak to withstand these conditions.

Adsorption of safranin O after 1h on NiO was very similar for nanoparticles and PBM (2.6 +/–1.7 vs. 2.9 +/–0.9 µg mg^{-1}), however, methylene blue adsorption on TiO_2 PBM was higher than on nanoparticles (4.4 +/–0.7 vs. 0.8 +/–0.6 µg mg^{-1}). Ultrasonic cavitation is oxidizing and is known to convert FeO into Fe_2O_3[23] and to oxidise titania;[24] such a process may have increased the negative charge of the surface of TiO_2, whereas NiO is already highly negatively charged.[25] No change in photocatalytic activity was observed for TiO_2 or NiO PBM compared with dispersions of native nanopowders (Figure 2b,c). Repeated adsorption of methylene blue followed by UV catalysis of 18 µM MB in 1 hour for 20 cycles resulted in no change in catalytic activity of TiO_2 PBM. Phosphate glass coated xerogels (0.6 to 5 wt%), however, had reduced photocatalytitc rates

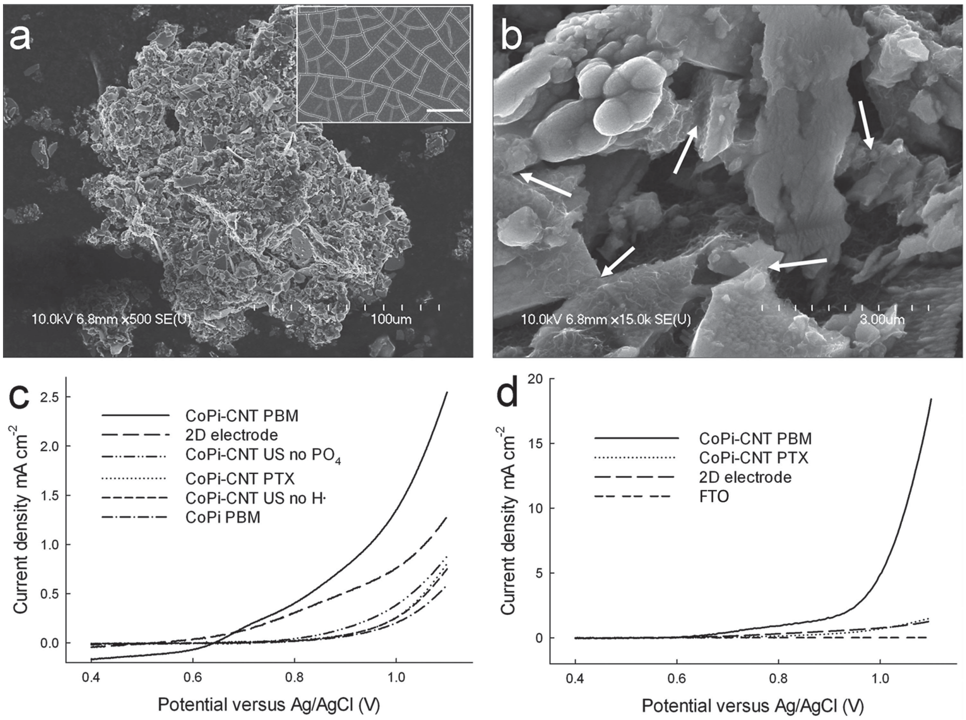

Figure 3. a) Scanning electron micrograph of CoPi-CNT PBM composite material used to construct the 3D electrode, insert shows electrodeposited Co catalyst on FTO glass (scale bar 5 μm). b) High magnification detail of CoPi-CNT PBM showing the intimate contact of the CoPi particles and CNT (arrows). c) Polarization curves showing the current densities generated as a function of applied potential for materials deposited onto FTO coated glass, the mass of deposited material was normalized to that present on the 2D electrode control at a scan rate of 10 mV s^{-1} in 0.1 M potassium phosphate buffer (pH 7.0). There was a reduction in current density for self-assembled CoPi catalyst (CoPi PBM) compared to electrodeposited 2D electrode controls. However, there was a large (ca. 2.5 times) increase in current density when Co was self assembled with CNT (CoPi-CNT PBM). This increase in activity was found to be dependent on ultrasound treatment and composite formation with CNT, since CoPi-CNT PTX achieved only moderately higher current densities to CoPi PBM; similarly when a H· scavenger was added during the ultrasound mediated self assembly process (CoPi-CNT US No H·), or additional phosphate was not added to the preparation (CoPi-CNT No PO$_4$) only a minor increase in catalytic activity was observed. d) Oxygen evolution voltammetry curves of 3D electrodes formed using CoPi-CNT PBM compared with electrodeposited 2D electrode control resulted in a ca. 15 times increase in current density at an applied potential of 1.1 V vs Ag/AgCl. In comparison only a moderate increase in current density was achieved when CoPi catalyst was mixed with CNT without ultrasound treatment (CoPi-CNT PTX) indicating poor electrical contact between the composite components. The background electrochemical activity of the FTO substrate was insignificant.

of between 30 to 70% (Figure S7), suggesting that the 3 wt% phosphate in PBM was not predominantly present as a glass.

The translation of nanoscale materials into the 3rd dimension is challenging[26] and prevents the development of volume-efficient devices. Recently, an electrodeposited cobalt phosphate (CoPi) catalyst was reported with the lowest water oxidation potential ever revealed at pH 7.[13a,13b,27] We were able to process this hydrated material (10.5 wt% weight loss from 110–400 °C) into conductive CoPi-CNT PBM composites of approximately 200 μm in diameter (**Figure 3**a,b). Using a fixed area of fluorine doped tin oxide (FTO) coated glass electrode, current density with respect to water oxidation indicating oxygen evolution reaction (OER) for a conventional 2D electrodeposited electrocatalyst was compared with a 1 mm thick 3D electrode made from CoPi-CNT PBM in a nafion polymer. A large (15 times) increase in OER was only observed for CoPi-CNT PBM and not simple admixtures of the components or CoPi PBM without CNT (Figure 3c,d). These results indicate that the conductive CNT phase enhanced electron transfer from the semiconducting CoPi phase to the FTO electrode in PBM by forming electrically conductive and intimate contacts between the CoPi particles. CoPi-CNT PBM electrodes achieved a 5 h oxygen evolution rate of 85.8 ± 5.2 compared to 36.2 ± 4.8 μmol O_2 cm^{-2} for conventional 2D electrodes (n = 3) in cobalt ion free phosphate buffer (pH 7) and no change in performance was detected after 6.5 h operation (Figure S9, Video S1). The inconsistency between electrochemical activity and oxygen evolution indicates that the rate limiting step may have been the oxygen–oxygen bond reaction to form oxygen molecules or the release of formed gas from the substrate.[14,28] Nevertheless, the applicability of this simple approach to improve the performance of many 2D nanomaterial systems is self-evident. As observed in our prior experiments, the absence of a phosphate coating or the addition of H· scavengers prevented CoPi-CNT PBM formation and also subsequent electrical contact between CoPi and CNT (Figure 3c).

Survey and high resolution XPS of TiO_2 and CoPi-CNT did not reveal speciation differences between PTX and PBM (Figure S10). Our data then indicate a very subtle change in surface chemistry had occurred during PBM formation. The

DOI: 10.1002/adma.201301818

increase in strength not being accompanied by an increase in density points to a change in the bond type between primary nanoparticles. The apparent involvement of $H\cdot$ radicals in this process is intriguing since very little is known about these extremely short lived (ca. 10^{-6}–10^{-7} s) species.[20] We postulate that the conditions created during bubble cavitation either on or in the air-filled PTX form phosphate radicals, the product of the phosphate ion oxidation, having a half-life of about 300 ps at room temperature.[29] These radicals could theoretically form phosphates and oxyphosphates at the surface of the PTX nanoparticles.[30] Covalent bonding of these phosphate surfaces at collision points between xerogel fragments with the potential to bridge nanoparticles might reasonably be expected given reports of mechano-[31] and ultrasonic[32] induced reaction of a variety of metal phosphates and oxyphosphates. The low levels of phosphate present frustrated characterization, but treatment with phosphatase solution at pH 7.4 and 9 selecting pyrophosphatase and phosphatase activities, respectively[33] did not cause any fragmentation of PBM, neither did treatment in either 1N HCl or 1N NaOH at 100 °C for 6 h, known to degrade linear and cyclical polyphosphates, or calcining to 300 °C for 2 h followed by immersion in water. These data seem to reject the notion of phosphate glass fusion of nanoparticles being the cause of PBM and point towards considerable potential for using what we term ionic welding to manipulate nanoparticles into functional materials.

Although ultrasonic cavitation phenomena have been observed for decades and sonically generated radicals and cavitation are widely employed in chemical and particulate synthesis to good effect,[1,2,34] there has been little progress in capitalizing on the reportedly huge localized temperatures and associated radical formation to build new materials from particulate precursors. To the best of our knowledge this is the first time that the normally destructive forces of ultrasonic cavitation and associated radical formation have been applied to the microscale assembly of preformed nanoparticles whilst simultaneously retaining nanoscale functionality. The discovery of the interaction of surface adsorbed orthophosphate with cavitation events offers materials science a new tool for the creation of a multitude of new functional nanocomposites.

Experimental Section

Microparticle Synthesis and Self-Assembly: Titanium Dioxide nanopowder (Aeroxide P25 TiO_2, Ø ≈20 nm) was supplied by Evonik Industries (Parsippany, NJ), Tungsten nanopowder (W, 99.95+%, Ø 40–60 nm) was supplied by US Research nanomaterials Inc. (Houston, TX), Nickel (II) oxide nanopowder (NiO, Ø < 50 nm), carbon nanopowder (C, Ø < 50 nm) and carbon nanotubes (CNT, multiwalled, Ø 6–9 nm) were supplied by Sigma Aldrich Canada (Oakville, ON). All other chemicals used were of reagent grade or better and were supplied by Sigma Aldrich Canada, unless stated otherwise. Nanocrystalline hydroxyapatite ($Ca_{10}(PO_4)_6OH_2$, Ø < 40 nm) was precipitated following the method of Jarcho et al.[35] Silver nanoparticles were synthesized by slowly adding 1 mL 100 mM aqueous silver nitrate solution to 100 mL of boiling 7 mM sodium citrate solution at pH 7. The reaction was then refluxed for 30 minutes. Cobalt phosphate catalyst (CoPi) was formed following the method of Kanan et al.[13a] Briefly, catalyst films were electrodeposited on fluorine-doped tin oxide (FTO) electrodes (Pilkington TEC7 Glass™) by controlled potential electrolysis of a 0.5 mM $Co(NO_3)_2$ aqueous solution in 100 mM potassium phosphate buffer at pH 7.0. Electrolysis was performed at 0.85 V (vs. Ag/AgCl) for several hours depending on the desired catalyst film thickness. After deposition, the electrodes were rinsed with deionized water and allowed to air-dry before carefully removing and collecting the catalyst using a razor blade. Prior to mixing with CoPi particles, CNT were suspended in isopropyl alcohol (IPA) at a concentration of 1 mg mL^{-1} and sonicated for 5 minutes to thoroughly disperse them. Immediately afterwards an aliquot of this suspension was mixed with CoPi to give a final CNT concentration of 0.3 wt%.

In order to create PTX, Na_3PO_4 or H_3PO_4 solutions (Fisher Scientific and Sigma Aldrich Canada, respectively) were added to nanoparticulate powders in aqueous solution (0.025–3.33 mM g^{-1}). Assuming a P–O bond length of 150 pm[36] and a surface area for each surface of the PO_4 tetrahedron of 3×10^{-20} m^2, the relative surface coverage of PO_4^{3+} ions to the nanoparticulate powders was calculated and concentrations adjusted accordingly to give between 0.5–100% coverage. Following mixing, the pastes were dried at 100 °C to form a granular xerogel, which was then lightly crushed in a pestle and mortar to give the PTX starting material. PTX were then suspended in a range of solvents (water, isopropanol, acetic acid, toluene, DMSO) at a concentration of 0.5–10 wt/vol%. Typically water or IPA was used, having identified them as suitable, and treated with ultrasound using an unmodified benchtop ultrasonic bath (Branson UltraSonic Model 1510 MT, 42 kHz, 70 W) for times of 1–60 minutes. Microscale PBM were separated from unagglomerated nanoparticles by washing through a 53 μm sieve.

Supporting Information

Supporting Information is available from the Wiley Online Library or from the author.

Acknowledgements

Mr R. Roy (McGill University) for assistance with ICP-OES measurements. Prof. R. Hill (McGill University) for helpful discussions. Prof. G. P. Demopoulos (McGill University) for the use of a solar simulator. Prof. J. A. Finch (McGill University) for the loan of a potentiostat. Pilkington Glass Ltd. for a generous donation of FTO glass. Supported by NSERC Nano IP award (D.C.B.), NSERC Discovery Grant, NSERC Strategic Grant, Canada Foundation for Innovation and Canada Research Chair (J.E.B.)

Received: April 23, 2013
Revised: May 25, 2013
Published online:

---

[1] N. K. Bourne, *Shock Waves* **2002**, *11*, 447–455.
[2] a) J. H. Bang, K. S. Suslick, *Adv. Mater.* **2010**, *22*, 1039–1059; b) D. G. Shchukin, E. Skorb, V. Belova, H. Mohwald, *Adv. Mater.* **2011**, *23*, 1922–1934.
[3] a) S. Sharifi, S. Behzadi, S. Laurent, M. L. Forrest, P. Stroeve, M. Mahmoudi, *Chem. Soc. Rev.* **2012**, *41*, 2323–2343; b) M. J. McCall, *Nat. Nanotechnol.* **2011**, *6*, 613–614; c) C. L. S. Wiseman, F. Zereini, *Sci. Total Environ.* **2009**, *407*, 2493–2500.
[4] T. Valdes-Solis, A. B. Fuertes, *Mater. Res. Bull.* **2006**, *41*, 2187–2197.
[5] G. W. Scherer, D. M. Smith, *J. Non-Cryst. Solids* **1995**, *189*, 197–211.
[6] K. E. Parmenter, F. Milstein, *J. Non-Cryst. Solids* **1998**, *223*, 179–189.
[7] N. Leventis, C. Sotiriou-Leventis, G. H. Zhang, A. M. M. Rawashdeh, *Nano Lett.* **2002**, *2*, 957–960.
[8] Y. Q. Wang, X. H. Tang, L. X. Yin, W. P. Huang, Y. R. Hacohen, A. Gedanken, *Adv. Mater.* **2000**, *12*, 1183–1186.
[9] a) S. J. Doktycz, K. S. Suslick, *Science* **1990**, *247*, 1067–1069; b) T. Prozorov, R. Prozorov, K. S. Suslick, *J. Am. Chem. Soc.* **2004**,

126, 13890–13891; c) D. Radziuk, D. Grigoriev, W. Zhang, D. Su, H. Möhwald, D. Shchukin, *J. Phys. Chem. C* **2010**, *114*, 1835–1843.

[10] P. Buffat, J. P. Borel, *Phys. Rev. A* **1976**, *13*, 2287–2298.

[11] S. Ramesh, Y. Koltypin, A. Gedanken, *J. Mater. Res.* **1997**, *12*, 3271–3277.

[12] N. Enomoto, S. Maruyama, Z. Nakagawa, *J. Mater. Res.* **1997**, *12*, 1410–1415.

[13] a) M. W. Kanan, D. G. Nocera, *Science* **2008**, *321*, 1072–1075; b) M. W. Kanan, Y. Surendranath, D. G. Nocera, *Chem. Soc. Rev.* **2009**, *38*, 109–114; c) S. Cobo, J. Heidkamp, P. A. Jacques, J. Fize, V. Fourmond, L. Guetaz, B. Jousselme, V. Ivanova, H. Dau, S. Palacin, M. Fontecave, V. Artero, *Nat. Mater.* **2012**, *11*, 802–807.

[14] Y. Surendranath, M. W. Kanan, D. G. Nocera, *J. Am. Chem. Soc.* **2010**, *132*, 16501–16509.

[15] a) A. G. Evans, M. E. Gulden, M. Rosenblatt, *Proc. R. Soc. London Ser. A-Math. Phys. Eng. Sci.* **1978**, *361*, 343–365; b) J. G. Chacon-Nava, F. H. Stott, S. D. de la Torre, A. Martinez-Villafane, *Mater. Lett.* **2002**, *55*, 269–273.

[16] L. Duffours, T. Woignier, J. Phalippou, *J. Non-Cryst. Solids* **1995**, *186*, 321–327.

[17] T. Terao, T. Nakayama, *Phys. Rev. E* **1998**, *58*, 3490–3494.

[18] E. C. D. Lima, F. Galembeck, *J. Colloid Interface Sci.* **1994**, *166*, 309–315.

[19] S. Koda, T. Kimura, T. Kondo, H. Mitome, *Ultrason. Sonochem.* **2003**, *10*, 149–156.

[20] R. Roots, S. Okada, *Radiat. Res.* **1975**, *64*, 306–320.

[21] J. Rae, M. Ashokkumar, O. Eulaerts, C. von Sonntag, J. Reisse, F. Grieser, *Ultrason. Sonochem.* **2005**, *12*, 325–329.

[22] I. S. Kulaev, V. M. Vagabov, T. V. Kulakovskaia, *The biochemistry of inorganic polyphosphates*, J. Wiley, Chichester, UK **2004**.

[23] E. Kowalska, J. Mizera, *Przem. Chem.* **1969**, *48*, 210–212.

[24] N. Sakai, R. Wang, A. Fujishima, T. Watanabe, K. Hashimoto, *Langmuir* **1998**, *14*, 5918–5920.

[25] N. Hernández, R. Moreno, A. J. Sánchez-Herencia, J. L. G. Fierro, *J. Phys. Chem. B* **2005**, *109*, 4470–4474.

[26] R. K. Joshi, J. J. Schneider, *Chem. Soc. Rev.* **2012**, *41*, 5285–5312.

[27] Y. Surendranath, M. Dinca, D. G. Nocera, *J. Am. Chem. Soc.* **2009**, *131*, 2615–2620.

[28] a) Y. Surendranath, *Ph.D. Thesis*, Massachusetts Institute of Technology, USA **2011**; b) J. Jirkovský, M. Makarova, P. Krtil, *Electrochem. Commun.* **2006**, *8*, 1417–1422.

[29] J. R. Huber, E. Hayon, *J. Phys. Chem.* **1968**, *72*, 3820–3827.

[30] Y. C. Tang, X. H. Huang, H. Q. Yu, L. H. Tang, *Int. J. Photoenergy* **2012**.

[31] M. N. Kislitsyn, A. B. Yaroslavtsev, *Solid State Ionics* **2003**, *162*, 197–202.

[32] Y. Y. Fan, Z. C. Hu, J. Yang, C. Zhang, L. Zhu, *Appl. Surf. Sci.* **2013**, *266*, 22–26.

[33] a) Y. Xu, T. F. Cruz, K. P. Pritzker, *J. Rheumatol.* **1991**, *18*, 1606–1610; b) A. Mizutani, R. J. Barrnett, *Nature* **1965**, *206*, 1001–1003.

[34] a) C. E. Brennen, *Cavitation and bubble dynamics*, Oxford University Press, New York, USA **1995**; b) K. S. Suslick, G. J. Price, *Annu. Rev. Mater. Sci.* **1999**, *29*, 295–326.

[35] M. Jarcho, C. H. Bolen, M. B. Thomas, J. Bobick, J. F. Kay, R. H. Doremus, *J. Mater. Sci.* **1976**, *11*, 2027–2035.

[36] B. Gamoke, D. Neff, J. Simons, *J. Phys. Chem. A* **2009**, *113*, 5677–5684.